Low-frequency Vibrational Dynamics of Amorphous and Crystalline Silica

Peter W. Albers[a], Günther Michael[b], Hans Lansink Rotgerink[b], Martin Reisinger[b], and Stewart F. Parker[c]

[a] AQura GmbH, Rodenbacher Chaussee 4, D-63457 Hanau, Germany
[b] Evonik Industries AG, Business Unit Inorganic Materials, Rodenbacher Chaussee 4, D-63457 Hanau, Germany
[c] STFC Rutherford Appleton Laboratory, ISIS Facility, Chilton, Didcot, Oxfordshire, OX11 0QX, United Kingdom

Reprint requests to Dr. Peter Albers. Fax: +49 6181 59 3554. E-mail: peter.albers@aqura.de

Z. Naturforsch. **2012**, *67b*, 1016 – 1020 / DOI: 10.5560/ZNB.2012-0110
Received April 27, 2012

Dedicated to Professor Heribert Offermanns on the occasion of his 75th birthday and on the occasion of the 70th birthday of AEROSIL®

Crystalline silica shows strong, sharp signals at about 77 and 130 cm^{-1} in the inelastic neutron scattering spectrum that are missing or strongly different, broadened and shifted to lower frequency for the case of precipitated and fumed silica. The presence or absence of these signals is a sensitive signature of crystallinity or amorphicity in silica. The low-frequency phonon density of states of precipitated and fumed silica is typical for completely amorphous materials. This observation is in perfect agreement with data from X-ray diffraction and high-resolution transmission electron microscopy. The amorphicity is retained during granulation post-treatments.

Key words: Silica, Amorphous, Crystalline, Vibrational Density of States

Introduction

The vibrational modes of silicas have been investigated in detail by infrared (IR) spectroscopy. Especially the O–H stretching modes of isolated, geminal or vicinal silanol groups of different oxygen coordination are the focus, *e.g.*, of catalyst research and materials science [1, 2, and refs. cited therein]. The aim of the present study is to complement the large body of existing work on silicas by using inelastic incoherent neutron scattering (IINS) on the spectrometers TFXA (Time Focused Crystal Analyzer) and TOSCA (Thermal Original Spectrometer with Cyclindrical Analyzers) [3] at $T < 20$ K sample temperature to probe the very far infrared region. IINS data of crystalline and of amorphous precipitated and fumed silicas are compared, together with the results of high-resolution transmission electron microscopy (HR-TEM) images.

Due to the high penetrating power of the neutron [3, 4] large quantities (up to the hundred-gram scale) of silica can be probed completely in a single experiment. The transparency of silica to neutrons means that integral material properties become accessible, whereas data from IR spectroscopy are restricted to the surface regions of solids.

The large incoherent cross section of the proton (^{1}H, 79.8 barns, most other elements have a cross section < 5 barns) means that in IINS spectroscopy strong vibrational signals are measured for hydrogen-containing structural entities. The signal intensity also depends on the amplitude of motion, and therefore the observed spectrum represents an amplitude-weighted phonon density of states. Consequently, the detection of the well-known O–H valency vibrations which are of low amplitude is difficult in IINS, whereas low-frequency torsional and deformational modes appear with high intensity. These are the focus of the present study.

Experimental

Materials

As an example for typical bulk pieces of crystalline silica two lots of 4 – 8 mm sized sieve fractions of pebbles

were washed thoroughly with superpure water and dried at 378 K for 12 h. As examples for amorphous, finely divided, fluffy silicas, commercial precipitated ULTRASIL® 7000 and fumed AEROSIL® 200 and 380 (Evonik Industries AG) were used. The materials from flame production technology were measured as received, the precipitated silica after drying at 378 K for 12 h. The influence of additional post-treatments in the course of producing pelletized SiO_2 catalyst supports by wet agglomeration at room temperature, calcination at $T < 1250$ K in an oven and subsequent pelletization was studied on AEROSIL® 380. The nitrogen surface areas were $< 2\,m^2\,g^{-1}$ for the crystalline and 190 (ULTRASIL®) and 205 and $360\,m^2\,g^{-1}$ (AEROSIL® products) for the amorphous silicas in the original state.

High-resolution transmission electron microscopy, HR-TEM

Ground pieces of particles of the crystalline SiO_2 were dusted onto standard TEM-sample holders (200 mesh copper grids, coated with Holey Carbon foil). The aggregates of fumed and precipitated silica were dispersed in isopropanol/water, treated in an ultrasonic bath for three minutes and afterwards transferred onto the Holey Carbon foil using Eppendorff pipettes. A Jeol 2010F HR-TEM was operated at 200 keV primary electron beam energy.

Inelastic incoherent neutron scattering, IINS

The IINS spectra were recorded using the TFXA spectrometer and its successor, the TOSCA spectrometer, at the spallation neutron source ISIS of the Rutherford Appleton Laboratory, Chilton (U. K.) [3]. The samples were sealed into thin-walled aluminum cans (wall thickness < 0.5 mm) and evacuated by a turbomolecular pump. Sample sizes were in the range 30 – 90 g for the powder-type silicas and 170 g for the crystalline silica. Due to the high penetrating power of neutrons, large quantities of silica can be measured to obtain macroscopic, representative results on materials properties. A sample was quenched with liquid nitrogen to 77 K followed by cooling to $T < 20$ K using a closed-cycle helium cryostat. IINS on spectrometers like TFXA and TOSCA complements data from IR and Raman spectroscopies. Vibrational spectroscopy in the range of $18 - 2000\,cm^{-1}$ can be carried out. The spectra have been normalized to 1 g SiO_2, thus relative intensities are directly comparable.

Results and Discussion

The HR-TEM images in Figs. 1A–C compare the typical structure of crystalline silica and amorphous silicas at high electron optical resolution. The corresponding IINS spectra are depicted in Figs. 2 – 4. The crystalline structure and *d*-spacings of the long-range

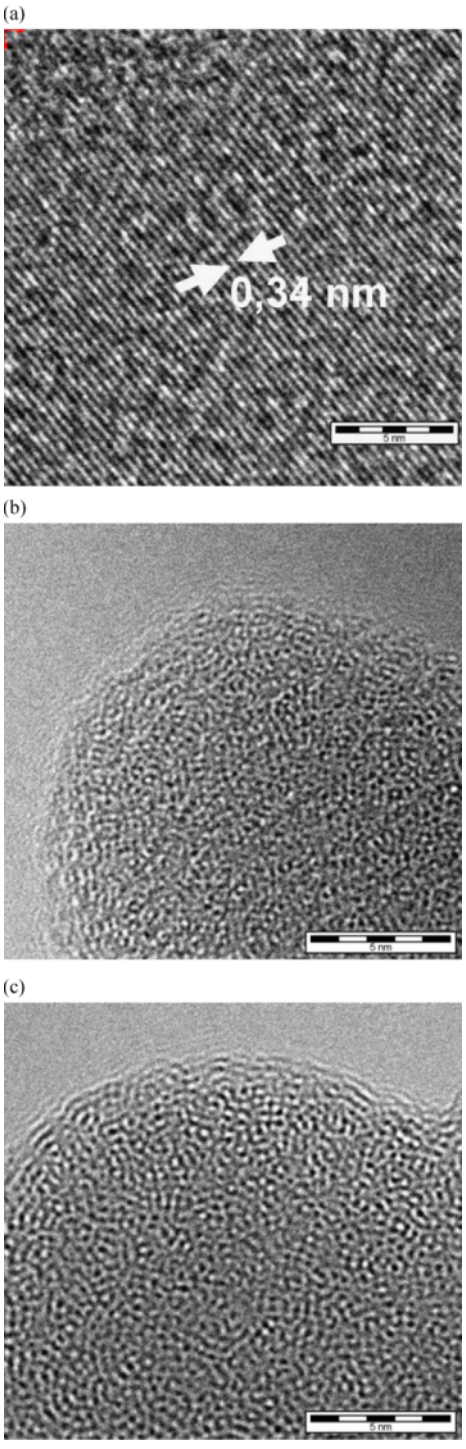

Fig. 1. HR-TEM images of crystalline and amorphous SiO_2. A: quartz; B: precipitated silica; C: fumed silica. Scale bars: 5 nm.

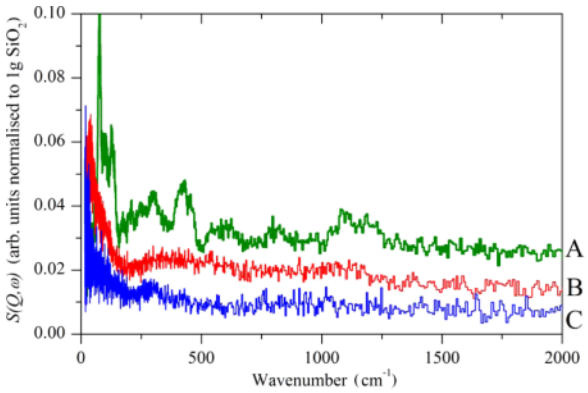

Fig. 2 (color online). IINS spectra of crystalline and of amorphous SiO_2. A: quartz; B: precipitated silica; C: fumed silica.

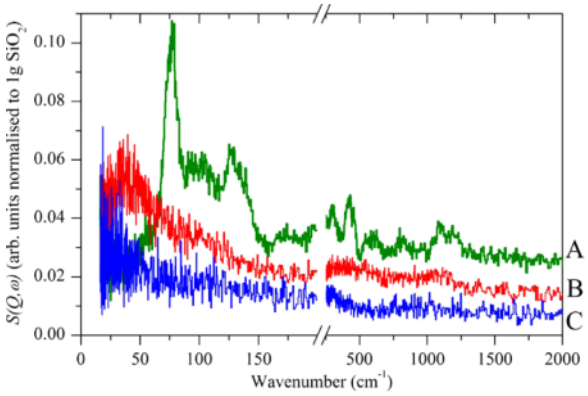

Fig. 3 (color online). Detailed regions of Fig. 2. Please note the strong low-energy bands for quartz (A) at *ca.* 77 and 130 cm^{-1} and their absence for precipitated (B) and fumed (C) silica.

ordered lattice are readily seen in Fig. 1 A including the *d*-spacing of quartz (0.34 nm for *hkl* 101). The HR-TEM images in Figs. 1B and C, however, illustrate the amorphous structure of the precipitated and the fumed silica. A three-dimensional network of randomly arranged SiO_4 tetrahedra with only short-range ordering is characteristic for these grades of silica.

A two-dimensional impression of the three-dimensional network of the interconnected SiO_4 entities is given by image contrast in the individual focus plane of a HR-TEM image. Such images directly support and complement the conclusions on amorphicity from previous X-ray diffraction work [5 – 7].

The IINS spectrum of the crystalline silica in Fig. 2A shows sharp, distinct vibrational bands. The higher-energy bands resemble the vibrational modes of HNa-Y zeolite which could previously be measured down to about 290 cm^{-1} [8, 9]. In Fig. 2A and, at expanded scale of the abscissa in the low frequency region, in Fig. 3A additional sharp low-frequency bands are observed at *ca.* 77 and 130 cm^{-1}. With respect to the high hydrogen selectivity of the IINS method it can be argued that the band at about 130 cm^{-1} can be due to a low frequency torsional movement of silanol groups. According to conclusions of Morrow and McFarlan a torsional mode of Si–OH can be expected at this energy [10]. Neutron scattering on vitreous silica led to the conclusion that bands at about 800 – 1200 cm^{-1} are due to Si–O stretching modes and those at 300 – 400 cm^{-1} to Si–O bending modes [11].

In the corresponding IINS spectra of the amorphous silica (Figs. 2B and C and, expanded, Figs. 3B and C) these sharp vibrational lines of the crystalline silica are either completely missing or strongly altered by distinct broadening and shifting towards very low energy ($< 60\ cm^{-1}$) to form a broad, low-frequency vibrational band. The IINS spectra typical of highly disordered amorphous materials are obtained [3, 11]. From the comparison of the spectra in Figs. 2 and 3 it follows that the three-dimensional network of the SiO_4 units of the fumed and of the precipitated silica is neither rigid and ordered enough to accommodate the sharp vibrational modes observed for crystalline silica, nor ideal

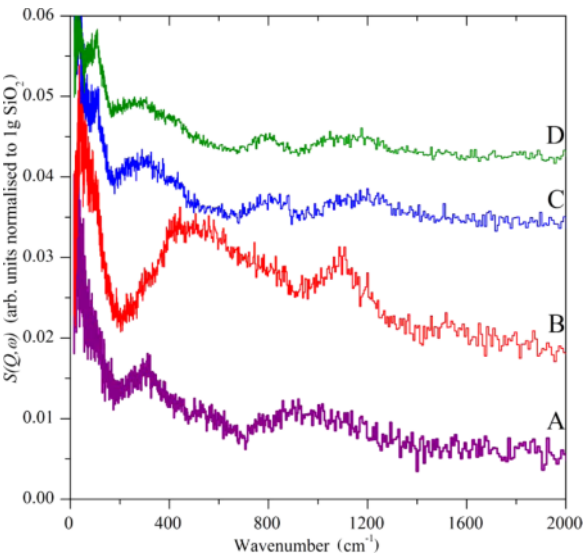

Fig. 4 (color online). IINS spectra of fumed silica. A: original, powder; B: agglomerated, wetted; C: calcined at $T <$ 1250 K; D: calcined and pelletized silica.

as calculated for glass-like SiO_2. According to calculations by Taraskin and Elliot [12], the vibrations of the SiO_4 units are expected to be composed of the rocking, bending and stretching contributions of Si–O–Si units in glass-like SiO_2 and to comprise a broad but sub-structured vibrational band spreading from about 65 – 940 cm^{-1} and a narrow double-structured band at about 1005 – 1340 cm^{-1}.

Figs. 4A–D illustrate the changes in the IINS spectrum of fumed silica in the course of wetting and agglomerating, calcination at $T < 1250$ K, and pelletization. For finely divided amorphous silica the calcination temperature is below the transition temperatures of the conversion of amorphous silica into the crystalline phases of quartz, tridymite or cristobalite: With increasing post-treatment temperature and compression treatment the finely divided X-ray-amorphous material exhibits slightly enhanced short-range structural ordering as indicated by slightly increasing contributions of the broad bands around 200 – 450, 700 – 900 and 1000 – 1300 cm^{-1}. The spectrum in Fig. 4B is dominated by the IINS spectrum of ice (note that the spectrum is recorded at $T < 20$ K) from the wetting and agglomerating treatment. Residual water is shock-frozen during the liquid nitrogen quench and is present as ice. Comparison with the neutron scattering spectra of the different phases of ice [13] and water-coated metal oxide nanoparticles [14 – 16] shows that the water molecules are present at the surface of the post-wetted silica as a highly disordered phase. Hydroxyls are also clearly present as shown by the band at ~1100 cm^{-1}.

In Figs. 4C and D the bands at 800 and 1000 – 1300 cm^{-1} that appear after calcination and pelletization of the fumed silica starting material somewhat resemble the phonon density of states of the three-dimensional network of SiO_4 entities according to the results of the calculations presented in [12]. In addition, a sharper feature around *ca.* 100 – 105 cm^{-1} starts to differentiate from the broad background of the amorphous starting material, whereas the sharp bands of crystalline silica at about 77 and 130 cm^{-1} (Fig. 2A) are still largely missing.

Table 1. Intensity ratio of the IINS bands at 77 and 130 cm^{-1}.

Sample / IINS Spectrometer used	Band ratio 77 cm^{-1}/130 cm^{-1}
Crystalline silica original sample 1 / TOSCA	1.63
Sample 1 after HF treatment / TOSCA	1.60
Sample 1 after D_2O treatment / TOSCA	1.78
Crystalline silica original sample 2 / TFXA	0.96

The numerical values in Table 1 illustrate the variation of the relative intensity of the 130 and the 77 cm^{-1} signals by lot-to-lot variation (samples 1 and 2), HF treatment (etching for increasing surface and silanol group density) or D_2O exchange. (Note that the total neutron scattering cross section of the deuteron (^2H) is only 7.64, less than 10 % of that of the proton. As a consequence, modes due to motions involving deuterons are usually not observed). This supports the interpretation of the 130 cm^{-1} band as being a silanol torsional mode because of the differences in silanol group densities (sample 1 and 2) and the presence of OH acidity (sensitivity to H/D exchange or HF treatment).

The phonon density of states for amorphous silica and for quartz has been calculated using the topology of a Bethe lattice [17] and further molecular dynamics simulations [18]. For amorphous silica a signal at around 70 cm^{-1} or less is known as the 'boson peak', and has been assigned as due to a high density of states related to the transversal acoustic phonon branch [19 – 21]. However, the assignment is still under debate [22, 23].

The identity of the ca. 77 cm^{-1} signal in crystalline silica is unresolved as well as the vibrational feature raising at around 100 – 105 cm^{-1} with increasing degree of structural ordering (Figs. 4C and D). The acoustic modes or torsions of the SiO_4 tetrahedra inside of the amorphous silica appear at significantly lower frequency (< 60 cm^{-1}) as a much broader band. The influence of hydrogen on the intensity of the low-energy vibrational modes of silica is also unresolved.

Conclusions

It is observed that crystalline SiO_2 (quartz) shows strong and sharp IINS signals at about 77 and 130 cm^{-1} which are missing or strongly different, broadened and shifted to lower frequency for the case of precipitated as well as fumed amorphous SiO_2. Experimental observation of these low-energy vibrational modes of silica which were already discussed and modelled in the literature for vitreous and amorphous grades of silica has not previously been achieved due to the low energy limits of other types of spectrometers.

Due to their high intensity in the crystalline material, the absence of these signals is indicative of, and a good signature of, amorphicity of silicas. The differences in the low-frequency vibrational dynamics illustrates strong differences between the rigid, ordered crystal lattice of quartz and the amorphous three-dimensional network of the SiO_4 tetrahedra in amorphous silicas.

Above 1400 cm^{-1}, infrared spectroscopy provides detailed information about the surface properties of silica, particularly regarding hydroxyl groups. However, silica is largely opaque to infrared radiation at energies $< 1400\,cm^{-1}$ because of the intense lattice absorption. The low energy vibrational bands of SiO_2 can be probed by IINS revealing the vibrational density of states of both surface species such as hydroxyls and also of the interior of the silica.

The low-frequency ($< ca.$ 150 cm^{-1}) phonon density of states of fumed and of precipitated silica is typical for completely amorphous materials. It is very similar for both, AEROSIL® and ULTRASIL®. This observation is in perfect agreement with data from X-ray diffraction [5 – 7] and high-resolution transmission electron microscopy (Fig. 1). The amorphicity is retained during granulation post-treatments.

Acknowledgement

The STFC Rutherford Appleton Laboratory is thanked for access to the neutron beam facilities.

[1] H. P. Boehm, H. Knözinger in *Catalysis – Science and Technology*, Vol. 4, (Eds.: J. R. Anderson, M. Boudart), Springer, Berlin, **1983**, pp. 39 – 207.
[2] P. Hoffmann, E. Knözinger, *Surf. Sci.* **1987**, *188*, 181 – 198.
[3] P. C. H. Mitchell, S. F. Parker, A. J. Ramirez-Cuesta, J. Tomkinson, *Vibrational Spectroscopy with Neutrons*, World Scientific, Singapore, **2005**, pp. 3; TFXA: pp. 100 – 193; TOSCA: pp. 104 – 108.
[4] P. W. Albers, S. F. Parker in *Advances in Catalysis*, Vol. 51, (Eds.: B. C. Gates, H. Knözinger), Academic Press, Amsterdam, **2007**, pp. 99 – 132.
[5] B. E. Warren, *Z. Kristallogr.* **1933**, *86*, 349 – 358.
[6] L. D. Evans, S. V. King, *Nature* **1966**, *212*, 1353 – 1354.
[7] O. W. Flörke, H. Graetsch, F. Brunk, L. Benda, S. Paschen, H. E. Bergna, W. O. Roberts, W. A. Welsh, D. M. Chapman, M. Ettlinger, D. Kerner, M. Maier, W. Meon, R. Schmoll, H. Gies, D. Schiffmann in *Ullmann's Encylopedia of Industrial Chemistry*, 6^{th} edition, Vol. 32, Wiley-VCH, Weinheim, **2003**, pp. 273 – 359. *Basic Characteristics of AEROSIL® Fumed Silica*, Technical Bulletin Fine Particles Number 11 (Ed. Evonik Industries, Applied Technology AEROSIL®), and literature cited therein.
[8] H. Jobic, *J. Catal.* **1991**, *131*, 289 – 293.
[9] W. P. J. H. Jacobs, J. H. M. C. Wolput, R. A. van Santen, H. Jobic, *Zeolites* **1994**, *14*, 117 – 125.
[10] B. A. Morrow, A. J. McFarlan, *J. Phys. Chem.* **1992**, *96*, 1395 – 1400.
[11] M. Arai, A. C. Hannon, A. D. Taylor, T. Otomo, A. C. Wright, R. N. Sinclair, D. L. Price, *Trans. Am. Cryst. Assoc.* **1991**, *27*, 113 – 131.
[12] S. N. Taraskin, S. R. Elliot, *Phys. Rev. B* **1997**, *56*, 8605 – 8622.
[13] J. C. Li, A. I. Kolesnikov, *J. Mol. Liq.* **2002**, *100*, 1 – 39.
[14] W. Dmowski, T. Egami, K. E. Swider-Lyons, C. T. Love, D. R. Rolison, *J. Phys. Chem. B* **2002**, *106*, 12677 – 12683.
[15] S. F. Parker, K. Refson, A. C. Hannon, E. Barney, S. J. Robertson, P. Albers, *J. Phys. Chem. C* **2010**, *114*, 14164 – 14172.
[16] E. C. Spencer, N. L. Ross, S. F. Parker, B. F. Woodfield, J. Boerio-Goates, S. J. Smith, R. E. Olsen, A. I. Kolesnikov, A. Navrotsky, C. Ma, *J. Phys.: Condens. Matter* **2011**, *23*, 205303 (6 pages).
[17] R. B. Laughlin, J. D. Joannopoulos, *Phys. Rev. B* **1977**, *16*, 2942 – 2952.
[18] J. Hörbach, W. Kob, K. Binder, *AIP Conf. Proc.* 479, **1998**, pp. 136 – 141.
[19] M. Grimsditch, A. Polian, R. Vogelsang, *J. Phys.: Condens. Matter* **2003**, *15*, S2335–S2341.
[20] M. J. Harris, M. T. Dove, J. M. Parker, *Mineral Mag.* **2000**, *64*, 435 – 440.
[21] V. L. Gurevitch, D. A. Parshin, H. R. Schober, *JETP Lett. Condens. Matter* **2002**, *78*, 553 – 557.
[22] A. I. Chumakov, G. Monaco, A. Monaco, W. A. Crichton, A. Bosak, R. Rüffer, A. Meyer, F. Kargl, L. Comez, D. Fioretto, H. Giefers, S. Roitsch, G. Wortmann, M. H. Maghnani, A. Hushur, Q. Williams, J. Balogh, K. Parlinski, R. Jochym, P. Piekarz, *Phys. Rev. Lett.* **2011**, *106*, 225501 – 225506.
[23] R. Zorn, *Physics* **2011**, *4*, 44 (3 pages).